Fabrication and characterization of ZnO:Sb/n-ZnO homojunctions

Ali Marzouki, Corinne Sartel, Nadia Haneche, Gilles Patriarche, Alain Lusson, Vincent Sallet, Meherzi Oueslati

Fabrication and characterizations of homojunctions n-ZnO/p-ZnO:Sb

Marzouki A.[*1] , C. Sartel[2], N. Haneche[2], G. Patriarche[3], A. Lusson[2], V. Sallet[2], M. Oueslati[1]

[1] Unité de Nanomatériaux et photonique, Faculté des Sciences de Tunis, Campus Universitaire, Elmanar, 2092 Tunis, Tunisie

[2] Université Paris-Saclay, CNRS, Université de Versailles St Quentin en Yvelines, Groupe d'Etude de la Matière Condensée (GEMAC), 45 avenue des Etats-Unis, Versailles 78035, France.

[3] Université Paris-Saclay, CNRS, Centre de Nanosciences et de Nanotechnologies (C2N), 10 Boulevard Thomas Gobert, Palaiseau 91120, France

e-mail: ali.marzouki@fst.utm.tn

Abstract:

Antimony doped ZnO layers have been grown by metal-organic vapor phase epitaxy on sapphire and ZnO substrates at high temperature (950°C) and low-pressure conditions (50 torr). Nitrous oxide and diethyl-zinc have been used as oxygen and zinc precursors, respectively. The incorporation of antimony has been obtained from the decomposition of triethyl-antimony doping molecules added in the gas phase. Sb concentrations were measured from 8.10^{18} to 10^{19} at /cm^{-3} using secondary ion mass spectroscopy. Our results suggest the formation of acceptor dopant-defect complexes, such as the Sb_{Zn}-$2V_{Zn}$. Low temperature photoluminescence spectra of Sb-doped layers exhibit donor-acceptor pair transitions at 3.253 eV. Unlike Raman spectra of nitrogen doped ZnO layers which show several local vibrational modes related to nitrogen incorporation, these modes which are absent in the antimony-doped ZnO layers. n-ZnO/p-ZnO:Sb homojunction diodes on ZnO substrate have been successfully elaborated. The current-voltage characteristics of the device exhibit a rectifying behaviour with a turn-on voltage of 3V.

Keywords : ZnO, MOVPE, triethyl-antimony, thin films, antimony doping, photoluminescence, SIMS, diode.

* E-mail: ali.marzouki@fst.utm.tn

1. Introduction

ZnO is a wide direct band gap semiconductor (Eg = 3.37 eV). Its large exciton binding energy (60 meV) at room temperature it one of the most promising candidates for the next generation of short-wavelength light emitting diodes (LEDs) and lasing devices [1-2]. However, the main obstacle to the realization of these components is the absence of an effective method that allows for p-type doping in a controllable manner. Many research have been conducted to achieve p-type doping in ZnO with group-V elements through various growth methods [3-7], such as molecular beam epitaxy (MBE) [813], pulsed laser deposition [14], magnetron sputtering [15-18], ion implanted [19-22] and metalorganic vapor phase epitaxy (MOVPE) [23-24]. Among these techniques, metalorganic vapour phase epitaxie processes have an obvious advantage for future industrialization. In this technique, metalorganic doping source is more controllable than inorganic doping gases [25]. Consequently, it is necessary to exploit an effective metalorganic source for p-type ZnO doping. In previous works, it has been reported experimentally and theoretically [15-27], that Sb could be an effective acceptor impurity in ZnO. In that sense, commercialized metalorganic compounds of Sb with less toxicity, such as trimethyl antimony (TMSb) and triethyl antimony (TESb) can be used.

In this work, antimony doped ZnO layers and p-ZnO:Sb/n-ZnO diode structures were fabricated by metalorganic vapour phase epitaxie using TESb as the doping source. Sb concentration was measured by SIMS. The samples, grown on sapphire and ZnO substrates, were characterised by Raman spectroscopy and photoluminescence (PL). I-V measurements were carried out on the diode structures after deposition of metallic contacts.

2. Experimental procedures

Diethyl zinc and nitrous oxide N_2O were used as zinc and oxygen precursors, respectively, and the carrier gas was helium. Growth temperature was set at 950°C and pressure of the metalorganic vapour phase epitaxie horizontal reactor was set at 50 torr [27]. Antimony doping was achieved using triethyl antimony (TESb) fluxes of 4 µmol/mn and 1 µmol/mn (series of samples labeled E_1 and E_2, respectively). The growth of these samples was carried out on different substrate: ZnO (O), and oriented sapphires M (10-10), R (1-102), A (11-20), C (0001). Each series includes five samples made under the same growth conditions deposited on different substrate.

To achieve the diode structure, the expected p-type ZnO: Sb layer (1.1 µm thick) was grown on top of the n-type ZnO substrate (500µm thick). To measure the electrical properties of the ZnO diode, Au–Ni electrodes with a thickness of 110 nm were deposited on the ZnO: Sb layer by the conventional thermal evaporation technique and indium electrodes on the back side of the n-type ZnO substrate by the welding technique.

The antimony concentration was determined by secondary ionization mass spectroscopy (SIMS) technique (Cameca IMS-4F). The current-voltage (*I–V)* characteristics were measured using a curve tracer type 576 at room temperature. The photoluminescence (PL) measurements were carried out at low temperature (T = 4K) using the 334 nm argon UV laser line as excitation. Raman spectroscopy measurements were carried out at room temperature with a T64000 Horiba Jobin Yvon spectrometer equipped with a microscope in back-scattering configuration using 488 nm argon laser line as excitation.

Scanning transmission electron microscopy (STEM) observations were made on a JEOL 2200 FS microscope equipped with a geometric aberration corrector on the probe. Thinned samples were prepared by focused ion beam technique after surface coating with Pt/C.

3. Results and discussion

3.3. Antimony doping of ZnO film

Secondary ionization mass spectroscopy （SIMS) measurement results are gathered in table 1 and show that antimony is well incorporated into ZnO up to some 10^{21} at.cm^{-3}. The incorporation of Sb in known to depends on the growth conditions such as TESb flux, temperature, growth rate and also the crystalline quality of the deposited material. In that sense, substrate nature and orientation is expected to have a major influence. The table 1 below compares the SIMS measurements for the two experiments, according to the nature of these substrates of ten samples: ZnO (O-face), and M, R, A, C oriented sapphires. It is observed that the epitaxial layers on sapphire R are too resistive to be analyzed by SIMS. For the other substrates, we notice a strong incorporation of antimony on sapphire M, A or C, up to 10^{21} at.cm^{-3}, compared to the case of homoepitaxy on ZnO(O) (~10^{19} at.cm^{-3}). The highest concentration is at the interface with the substrate. The growth rate is similar in all these samples.

Series	Samples	ZnO:Sb/ZnO (O-face)	ZnO:Sb/ Sapphire C	ZnO:Sb/ Sapphire R	ZnO:Sb/ Sapphire A	ZnO:Sb/ Sapphire M
E_1 (950°C, TESb=4µmol/mn)	Concentration (at.cm^{-3})	1,3.10^{19}	2.10^{20} à 10^{21}	High resistive	8.10^{19} à 10^{21}	3.10^{20} à 10^{21}
	Thickness (nm)	610	620		660	610
E_2 (950°C, TESb=1µmol/mn)	Concentration (at.cm^{-3})	10^{19}	1,4 à 6.10^{20}	High resistive	0,5 à 2.10^{20}	1 à 3.10^{20}
	Thickness (nm)	610	640		610	520

Table 1: SIMS measurements of antimony concentrations on doped ZnO:Sb.

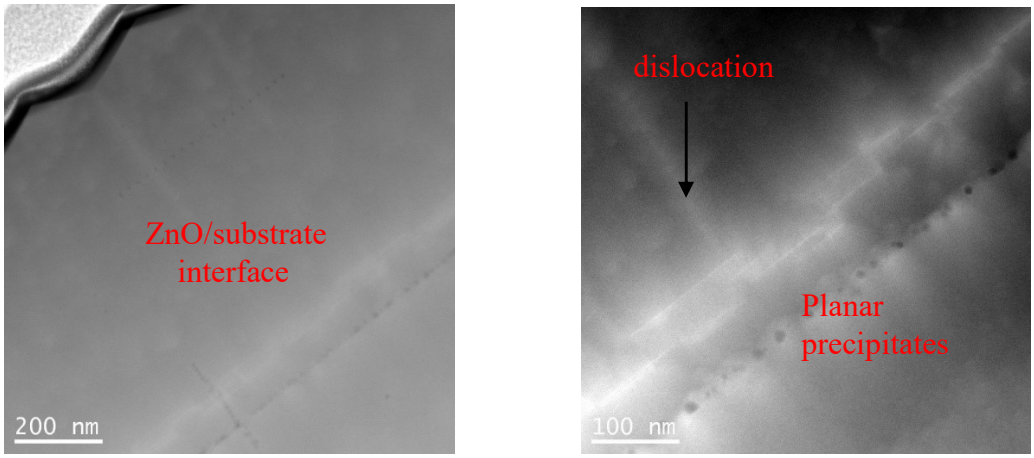

(a) **(b)**

Figure 1: STEM HAADF images of antimony-doped ZnO layer grown on substrate ZnO: (a) scale 200 nm and (b) 100 nm

The structural analysis of a homoepitaxial Sb-doped layer (ZnO:Sb/ZnO face-O) with a mean concentration of antimony about 10^{19} at.cm^{-3} was carried out by transmission electron microscopy. Although this is homoepitaxy, threading dislocations can be seen, and seem to be associated with the roughness of the surface (Figure 1a). In the zoom image (figure 1b) planar precipitates of Sb close to the interface are revealed. This explains the high levels of concentration [Sb] measured by SIMS at the film/substrate interfaces. In addition, a brighter chemical contrast is visible around the dislocations, showing a location of the dopant around these crystal defects. Thus, we deduce that the Sb content depends on the crystal defects, and it is suggested that the incorporation is partly related to dislocations and other structural defects 13]. Our observations are in agreement

with published works where the Sb_{Zn}-$2V_{Zn}$ complex is considered to be an acceptor, and structural defects facilitate its formation [28]. Hence, we do not expect to obtain p-type doping by substitution of the oxygen atom with antimony, but rather via this complex associating two vacancies of Zn to a antimony atoms in Zn sites.

3.2. Photoluminescence spectra:

Figure 2 shows the photoluminescence spectrum of the ZnO: Sb layer on sapphire. We observe the most convincing DAP (donor-acceptor pairs) transition, around 3.25 eV, accompanied by its two-phonon replicas. The transition related to stacking fault is seen at 3.32 eV [29], and thus reveals the presence of a high concentration of these structural defects in the layer. This observation agrees with the idea of an enhanced incorporation and/or a favoured activity of antimony with certain types of defects.

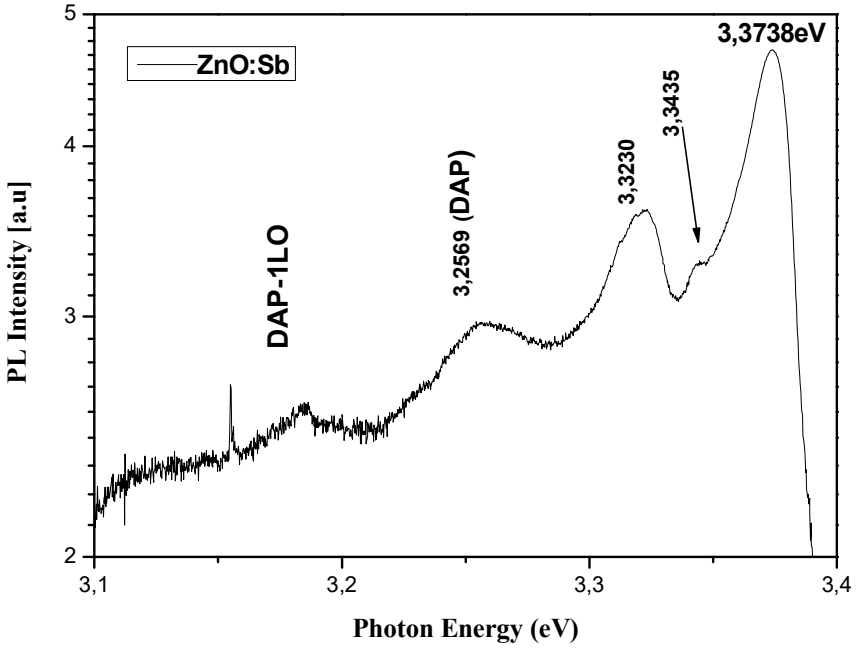

Figure 2: PL spectrum of a ZnO: Sb film on sapphire

3.3. Raman spectroscopy:

We report in Fig. 3 the room temperature Raman spectra of three different ZnO samples, namely undoped, (ZnO (ND) antimony doped (ZnO:Sb) and nitrogen doped (ZnO:N) measured in the wavenumber range from 100 to 1000 cm^{-1}. These spectra are dominated by the known strong peak E_2 mode (E_2^H) located at about 438 cm^{-1}. It is a characteristic of the wurtzite phase and represents the vibration of oxygen atoms [30, 32]. The feature at 332 cm^{-1}, which can be seen in the three spectra is a second-order Raman peak (E_2^H- E_2^L) of ZnO [29]. Similar Raman lines

located at 380 cm^{-1}, 410 cm^{-1} and 581.2 cm^{-1} are attributed to A_1 (TO), E_1 (TO) and A_1 (LO) ZnO Raman active modes, respectively [9, 31].

Moreover, an impurity, vacancy, interstitial or lattice distortion produces a disordered environment. The electron wave function spread in the k-space and electron–phonon interaction involves novel phonons of different wave vectors associated to impurity vibration and/or DATA (Disorder Activated Transversal Acoustic) and DALA (Disorder Activated Longitudinal Acoustic) Raman modes from the whole Brillouin zone. Then, in ZnO:N samples, additional Raman lines are observed at 275, 510, 582, and 643 cm^{-1}, and attributed respectively to additional modes related to nitrogen doping [33-34]. However, those peaks are not observed in undoped ZnO and in ZnO:Sb Raman spectra. In the case of ZnO:Sb sample, this could be explained by the big difference between Sb and N molar masses ($M_{Sb} >> M_N$). As the phonon frequency ratio Ω_N/Ω_{Sb} is proportional to $\sqrt{(M_{Sb}/M_N)}$, the additional Raman line at frequencies Ω_N = 275, 510, 582, and 643 cm^{-1} in ZnO:N (M_N=14) should be expected to appear in ZnO:Sb Raman spectrum in the frequency range [139 - 336 cm^{-1}]. In fact, the low frequency range in ZnO:Sb Raman spectrum is really different of that of ZnO:N and undoped ZnO spectra. Also, some other peaks associated to DATA and DALA modes appeared in this low frequency region due to the breaking down of the wave vector conservation law in the Raman scattering,

For a better comparison between these ZnO:Sb, ZnO:N and undoped ZnO samples, a fitting procedure of the Raman spectra in the low frequency range [100-300 cm^{-1}] is needed. Fig. 4 shows an example of mixed Lorentzian and Gaussian distribution fittings for those three samples. The fitted region is resolved into twelve peaks. The obtained phonon frequencies of the fitted region for the three films are shown in Table II. It is important to underline that certain criteria are necessary to have a better fit of the Raman spectrum. In the case of the undoped ZnO, the Raman spectrum has a wide band and a low signal/noise ratio which strongly affect the adjustment procedure. The low frequency region (100 - 300 cm-1 for ZnO). corresponds mainly to transverse acoustic phonons "TA" and longitudinal "LA" from the edges of the Brillouin zone. These modes are normally forbidden in first order Raman processes and therefore unobservable. The choice of

the number of peaks needed to adjust the lo w Raman frequency region depends on the number of observed Raman peaks associated to the combinations of double-phonon modes (2TA, 2LA, TA + LA, etc.) at the different points of the Brillouin zone. The fitted Raman spectra show:

i- Common peaks sited at about 103, 113 and 134 cm^{-1} which could be attributed to DATA and DALA ZnO modes.

ii- The peaks at [157 - 162], [200 - 211] and [271 - 292] cm^{-1} are mainly observed in doped ZnO:Sb and ZnO:N. They could be to additional modes due to doping impurities and also to residual impurities in undoped ZnO.

iii- The broadening bands at 134, 180 and 248 cm^{-1} are very large and couldn't be associated to Raman band. The incorporation of impurities into the material results the formation of deep localized states in the band gap. We attribute them to the optical transitions due to the interactions with phonons.

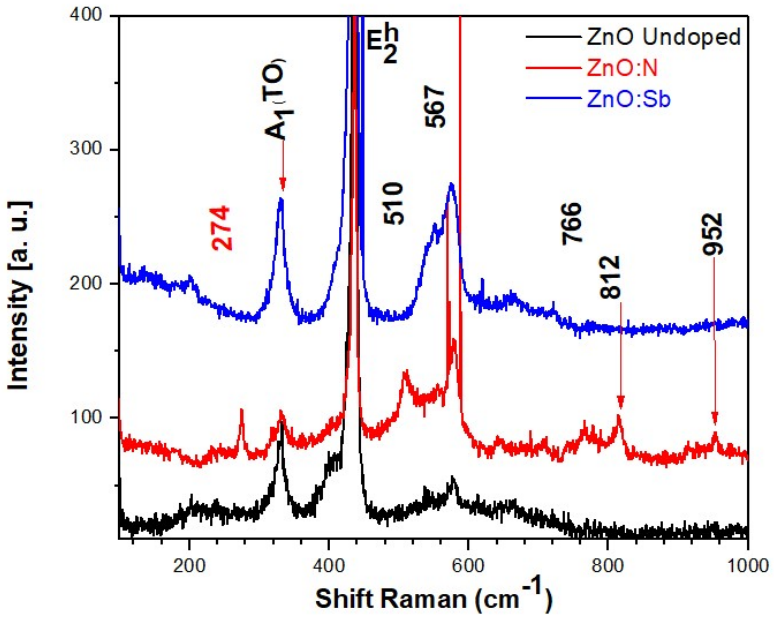

Figure 3: Raman spectra at room temperature of thin films of undoped ZnO and doped with antimony and nitrogen

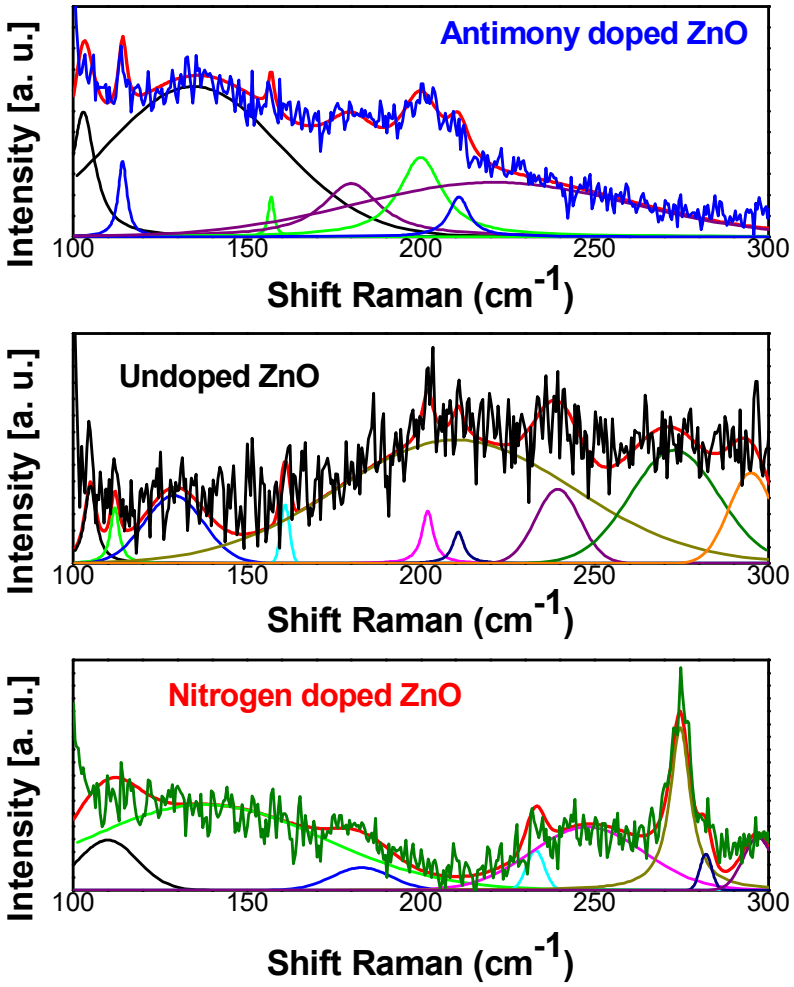

Figure 4: Raman spectra of ZnO (ND), (ZnO:Sb) and (ZnO:N), obtained at room temperature, in the range 100 cm^{-1} - 300 cm^{-1}. The spectra are fitted using Gaussian and Lorentzian sub-bands.

Sample	Additional modes (cm^{-1})
ZnO : Sb	E_2^1 103 113 134 157 180 200 211
ZnO :N	105 112 145 180 231 248 274 282 295
Undoped ZnO	105 112 130 162 202 211 238 271 292

Table 2. The observed additionnal modes in Sb, N doped and undoped ZnO thin films grown by MOVPE.

3.4. I (V) measurements on ZnO:Sb thin films :

To check the presence of an potential p-type in homoepitaxial ZnO: Sb films, we have realized a diode, with two Ni / Au contacts on the front doped layer, and indium back contacts on the

substrate. These contacts are used to measure the I (V) characteristic of the samples. The Ni / Au contact (10/100 nm) is deposited by thermal evaporation; without annealing [35, 46] whereas the indium contact is soldered on the back side. The schema of the structure is shown in figure 5.

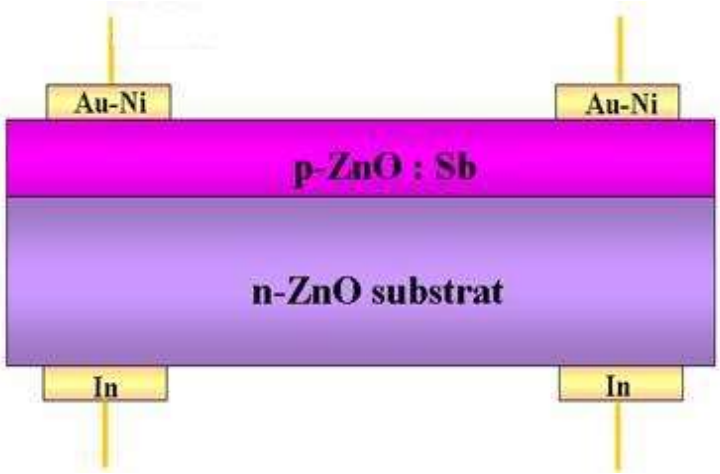

Figure 5: The diode structure

About ten samples were tested. Two of them showed rectifying characteristics between upper and lower contacts. We also took care to check the ohmicity between the two upper (Ni / Au) and lower (In) contacts.

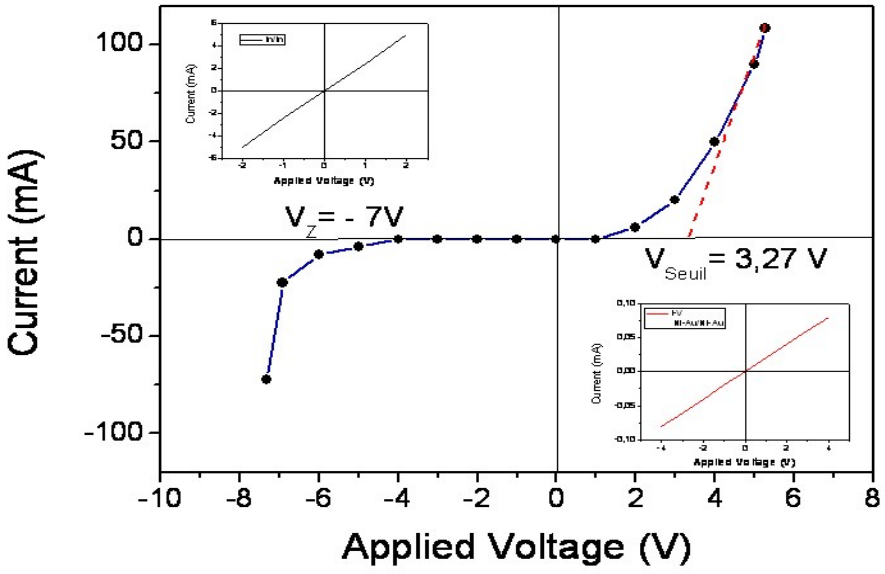

(a)

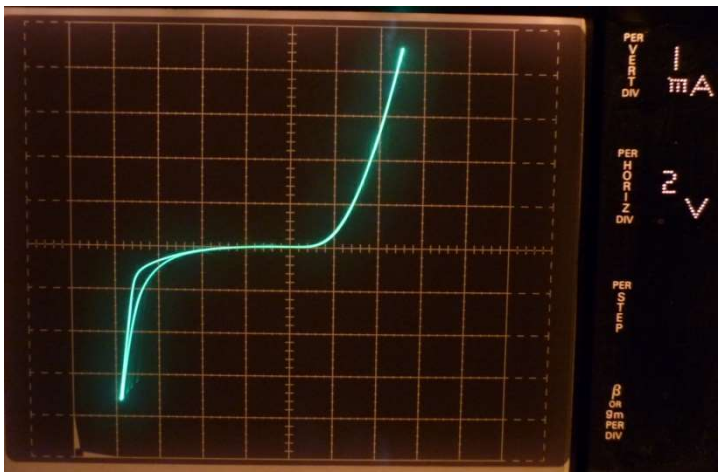

(b)

Figure 6: I (V) Characteristics of a ZnO Diode:a) curve ; b) Photo

The room temperature I-V curve of the (p-ZnO:Sb/n-ZnO) p–n homojunction diode is shown in figure 6. A clear rectifying behaviour of the ZnO p–n homojunction is demonstrated by the I–V curve. The forward turn-on voltage and reverse breakdown voltage are 3.27V. As shown in the inset of figure 6, the In n-type ZnO layer contact and the Au–Ni p-type ZnO:Sb layer contact both show a good ohmic behaviour and confirm that the rectification behaviour arises from the ZnO homojunction. These results further demonstrate the effective p-type conductivity of ZnO : Sb film [47-48].

4. Conclusion

Antimony doped ZnO films have been grown by MOVPE and characterized. We obtained a good incorporation of antimony into the ZnO up to some 10^{21} at.cm^{-3}. This incorporation depends on the growth conditions, and also on the crystalline quality of the deposited material. Our results suggests the formation of dopant-defects complexes, such as Sb_{Zn}-$2V_{Zn}$, rather than a substitution of the oxygen atom by antimony. This might be not a drawback. On the contrary, and according to published works, the Sb_{Zn}-$2V_{Zn}$ complex is an acceptor which appearance is related to the existence of structural defects. Our observations agree well with that. In particular, the layers deposited on sapphire exhibit the best DAP transitions in photoluminescence, densities of large stacking faults, and a high resistivity that could be related to residual n-type compensation by the acceptors. Finally, the I(V) characteristics of our p-ZnO:Sb/n-ZnO structures highlight that the Sb-doped ZnO layers are potentially p-type.

References

[1] Ü. Özgür, Y.I. Alivov, C. Liu, a Teke, M. a Reshchikov, Ü. Özgür, et al., A comprehensive review of ZnO materials and devices APPLIED PHYSICS REVIEWS A comprehensive review of ZnO materials and devices, Appl. Phys. 98, 041301. 041301 (2005). doi:10.1063/1.1992666.

[2] Sung-Doo Baek, Yun Cheol Kim, Jae-Min Myoung, Sb-doped p-ZnO quantum dots: Templates for ZnO nanorods homojunction white light-emitting diodes by low-temperature solution process, Applied Surface Science, 480 (2019) 122-130. https://doi.org/10.1016/j.apsusc.2019.02.209.[3] Sandhya Y. Wakhare, Mrinalini D. Deshpande, Structural, electronic and optical properties of metalloid element (B, Si, Ge, As, Sb, and Te) doped g-ZnO monolayer: A DFT study, Journal of Molecular Graphics and Modelling, 101 (2020) 107753.
https://doi.org/10.1016/j.jmgm.2020.107753

[4] S.B. Zhang, S.H. Wei, A. Zunger, Intrinsic n-type versus p-type doping asymmetry and the defect physics of ZnO, Phys. Rev. B - Condens. Matter Mater. Phys. 63 (2001) 1–7. doi:10.1103/PhysRevB.63.075205.

[5] J.M. Bian, X.M. Li, C.Y. Zhang, W.D. Yu, X.D. Gao, P-type ZnO films by monodoping of nitrogen and ZnO-based p-n homojunctions, Appl. Phys. Lett. 85 (2004) 4070–4072. doi:10.1063/1.1808229.

[6] J.Z. Zhao, H.W. Liang, J.C. Sun, J.M. Bian, Q.J. Feng, L.Z. Hu, et al., Electroluminescence from n-ZnO/p-ZnO : SSSSb homojunction light emitting diode on sapphire substrate with metal-organic precursors doped p-type ZnO layer grown by MOCVD technology, J. Phys. D. Appl. Phys. 41 (2008). doi:10.1088/0022-3727/41/19/195110.

[7] S. Limpijumnong, S.B. Zhang, S.H. Wei, C.H. Park, Doping by large-size-mismatched impurities: The microscopic origin of arsenicor antimony-doped p-type zinc oxide, Phys. Rev. Lett. 92 (2004) 1–4. doi:10.1103/PhysRevLett.92.155504.

[8] E. Przezdziecka, W. Lisowski, R. Jakiela, J.W. Sobczak, A. Jablonski, M.A. Pietrzyk, A. Kozanecki, Arsenic chemical state in MBE epitaxial grown ZnO layers - Doped with As, N and Sb, Journal of Alloys and Compounds, S0925-8388(16)31937-5.
http://dx.doi.org/10.1016/j.jallcom.2016.06.213

[9] K.M. Paradowska, E. Przeździecka, E. Płaczek-Popko, E. Zielony, M. Stachowicz, A. Kozanecki, Effect of annealing on photoluminescence and Raman scattering of Sb-doped ZnO epitaxial layers grown on a-Al2O3, Journal of Alloys and Compounds, S0925-8388(18)33644-2.
https://doi.org/10.1016/j.jallcom.2018.09.379

[10] L.J. Mandalapu, F.X. Xiu, Z. Yang, D.T. Zhao, J.L. Liu, P-type behavior from Sb-doped ZnO heterojunction photodiodes, Appl. Phys. Lett. 88 (2006) 1–4. doi:10.1063/1.2186516.

[11] L.J. Mandalapu, Z. Yang, S. Chu, J.L. Liu, Ultraviolet emission from Sb-doped p -type ZnO based heterojunction light-emitting diodes, Appl. Phys. Lett. 92 (2008) 3–5. doi:10.1063/1.2901018.

[12] S. Chu, J.H. Lim, L.J. Mandalapu, Z. Yang, L. Li, J.L. Liu, Sb-doped p-ZnOGa -doped n-ZnO homojunction ultraviolet light emitting diodes, Appl. Phys. Lett. 92 (2008) 1–3. doi:10.1063/1.2908968.

[13] W. Guo, a. Allenic, Y.B. Chen, X.Q. Pan, Y. Che, Z.D. Hu, et al., Microstructure and properties of epitaxial antimony-doped p-type ZnO films fabricated by pulsed laser deposition, Appl. Phys. Lett. 90 (2007) 242108. doi:10.1063/1.2747669.

[14] X.H. Pan, W. Guo, Z.Z. Ye, B. Liu, Y. Che, H.P. He, et al., Optical properties of antimony-doped p-type ZnO films fabricated by pulsed laser deposition, J. Appl. Phys. 105 (2009) 21–24. doi:10.1063/1.3126518.

[15] Chukwudi E. Iheomamere, Corey L. Arnold, Urmilaben P. Rathod, Khalil D. Omotosho, Andrey A. Voevodin, Nigel D. Shepherd, Bonding and stoichiometry in low-energy radio frequency magnetron sputtered ZnO thin films on flexible substrate, Vacuum, (2020) 109869. https://doi.org/10.1016/j.vacuum.2020.109869

[16] Muhammad Abiyyu Kenichi Purbayanto et al., Enhancement in green luminescence of ZnO nanorods grown by dc-unbalanced magnetron sputtering at room temperature, Optical Materials, 108 (2020) 110418.
https://doi.org/10.1016/j.optmat.2020.110418
[17] E. Przeździecka, E. Kamińska, I. Pasternak, a. Piotrowska, J. Kossut, Photoluminescence study of p -type ZnO:Sb prepared by thermal oxidation of the Zn-Sb starting material, Phys. Rev. B - Condens. Matter Mater. Phys. 76 (2007) 10–13. doi:10.1103/PhysRevB.76.193303.
[18] J.M. Qin, B. Yao, Y. Yan, J.Y. Zhang, X.P. Jia, Z.Z. Zhang, et al., Formation of stable and reproducible low resistivity and high carrier concentration p -type ZnO doped at high pressure with Sb, Appl. Phys. Lett. 95 (2009) 1–4. doi:10.1063/1.3153515.
[19] Avanendra Singh, K. Senapati, D.P. Datta, R. Singh, T. Som, S. Bhunia, D. Kanjilal, Pratap K. Sahoo, Synthesis of p–n junctions in ZnO nanorods by O+ ion implantation, Nuclear Instruments and Methods in Physics Research B, (2017) 03 048.
http://dx.doi.org/10.1016/j.nimb.2017.03.048
[20] Wanjun Li, Hong Zhang, Xiaoyu Zhang, Guoping Qin, Honglin Li, Yuanqiang Xiong, Lijuan Ye, Haibo Ruan, Cunzhu Tong, Chunyang Kong, Liang Fang, Non-axial NO-VZn Shallow Acceptor Complexes in Nitrogen Implanted p-type ZnO Thin Films, Applied Surface Science, S0169-4332(20)31925-5.
https://doi.org/10.1016/j.apsusc.2020.147168
[21] QingFen Jiang, MinJu Ying b, Jie Lian, Kai Dai, YuJun Shi, MingYang Wei, ChenLin Wang, Yu Zhang, Effects of Kr implanted O-polar ZnO thin films on structure and optical properties, Optical Materials, 105 (2020) 109867.
https://doi.org/10.1016/j.optmat.2020.109867
[22] U. Wahl, J.G. Correia, T. Mendoṇa, S. Decoster, Direct evidence for Sb as a Zn site impurity in ZnO, Appl. Phys. Lett. 94 (2009) 2007–2010. doi:10.1063/1.3159474.
[23] Yi Cheng, Xizhen Zhang, Li Che, Jixiang Chen, Bo Jing, Rulin Sun, Xixian Luo, Binding energy of Sb-related complex in p-doped ZnO film, Journal of Alloys and Compounds, 800 (2019) 219-223.
https://doi.org/10.1016/j.jallcom.2019.06.033
[24] W. Liu, S.L. Gu, J.D. Ye, S.M. Zhu, S.M. Liu, X. Zhou, et al., Blue-yellow ZnO homostructural light-emitting diode realized by metalorganic chemical vapor deposition technique, Appl. Phys. Lett. 88 (2006). doi:10.1063/1.2169908.
[25] W.K. Fong, K.K. Leung, C. Surya, Si doping of metal-organic chemical vapor deposition grown gallium nitride using ditertiarybutyl silane metal-organic source, J. Cryst. Growth. 298 (2007) 239–242. doi:10.1016/j.jcrysgro.2006.10.024.
[26] Vesna Ribic, Aleksander Recnik, Matej Komelj , Anton Kokalj, Zorica Brankovic, Mario Zlatovic, Goran Brankovic, New inversion boundary structure in Sb-doped ZnO predicted by DFT calculations and confirmed by experimental HRTEM, Acta Materialia, 199 (2020) 633-648.
https://doi.org/10.1016/j.actamat.2020.08.035
[27] S. Limpijumnong, S.B. Zhang, S.H. Wei, C.H. Park, Doping by large-size-mismatched impurities: The microscopic origin of arsenicor antimony-doped p-type zinc oxide, Phys. Rev. Lett. 92 (2004) 1–4. doi:10.1103/PhysRevLett.92.155504.
[27] G. Du, Y. Ma, Y. Zhang, T. Yang, Preparation of intrinsic and N-doped p -type ZnO thin films by metalorganic vapor phase epitaxy, Appl. Phys. Lett. 87 (2005) 1–3. doi:10.1063/1.2132528.
[28] S. Limpijumnong, S. B. Zhang, S.-H. Wei and C. H. Park, Phys. Rev. Lett. **92** (2004) 155504.
[29] M. Schirra, R. Schneider, a. Reiser, G.M. Prinz, M. Feneberg, J. Biskupek, et al., Acceptor-related luminescence at 3.314 eV in zinc oxide confined to crystallographic line defects, Phys. B Condens. Matter. 401-402 (2007) 362–365. doi:10.1016/j.physb.2007.08.188.
[30] Lee E C, Kim Y S, Jin Y G and Chang K J 2001 *Phys. B: Condens. Matter* **308** 912–5.

[31] Damen T C, Porto S P S and Tell B 1966 *Phys. Rev.* **142** 570 Calleja J M and Cardona M 1977 *Phys. Rev.* B **16** 3753.
[32] B. Yang, P. Feng, A. Kumar, R.S.Katiyar and M. Achermann Appl. Phys. **42** (2009) 195402.
[33] A. Kaschner, U. Haboeck, Martin Strassburg, Matthias Strassburg, G. Kaczmarczyk, A. Hoffmann, C. Thomsen, A. Zeuner, H. R. Alves, D. M. Hofmann, and B. K. Meyer, Appl. Phys. Lett. **80**, 1909 (2002).
[34] L. L. Kerr, X.Li, M.Canepa, A.J.Sommer, Thin Solid Films **515**, 5282 (2007).

[35] K. Ip, G. T. Thaler, H. Yang, S. Y. Han, Y. Li, D. P. Norton, S. J. Pearton, S. Jang and F. Ren, J. Crys. Growth, **287** (2006) 149-156
[36] W. Mtangi, F.D. Auret, C. Nyamhere, P.J. Janse van Rensburg, a. Chawanda, M. Diale, et al., The dependence of barrier height on temperature for Pd Schottky contacts on ZnO, Phys. B Condens. Matter. 404 (2009) 4402–4405. doi:10.1016/j.physb.2009.09.022.
[37] P. Bhattacharyya, P.K. Basu, C. Lang, H. Saha, S. Basu, Noble metal catalytic contacts to sol-gel nanocrystalline zinc, Properties of arsenic-doped p-type ZnO grown by hybrid beam deposition, Appl. Phys. Lett. 83 (oxide thin films for sensing methane, Sensors Actuators, B Chem. 129 (2008) 551–557. doi:10.1016/j.snb.2007.09.001.
[38] Y.R. Ryu, T.S. Lee, H.W. White 2003) 87–89. doi:10.1063/1.1590423.
[39] H.S. Yang, Y. Li, D.P. Norton, K. Ip, S.J. Pearton, S. Jang, et al., Low-resistance ohmic contacts to p-ZnMgO grown by pulsed-laser deposition, Appl. Phys. Lett. 86 (2005) 1–3. doi:10.1063/1.1925309.
[40] Z.P. Shan, S.L. Gu, S.M. Zhu, W. Liu, K. Tang, H. Chen, et al., Rapid thermal annealing induced changes on the contact of Ni/Au to N-doped ZnO, Appl. Surf. Sci. 254 (2008) 6962–6966. doi:10.1016/j.apsusc.2008.05.118.
[41] J.H. Park, T.H. Kim, N.Y. Chang, J.S. Kim, G.H. Kim, B.T. Lee, Microstructural investigation of Ti/Au ohmic contacts on Ga doped single crystalline n-ZnO films, Mater. Sci. Eng. B Solid-State Mater. Adv. Technol. 167 (2010) 51–54. doi:10.1016/j.mseb.2010.01.026.
[42] S.S. Lin, J.G. Lu, Z.Z. Ye, H.P. He, X.Q. Gu, L.X. Chen, et al., p-type behavior in Na-doped ZnO films and ZnO homojunction light-emitting diodes, Solid State Commun. 148 (2008) 25–28. doi:10.1016/j.ssc.2008.07.028.
[43] Z.Z. Zhang, Z.P. Wei, Y.M. Lu, D.Z. Shen, B. Yao, B.H. Li, et al., p-Type ZnO on sapphire by using O2-N2co-activating and fabrication of ZnO LED, J. Cryst. Growth. 301-302 (2007) 362–365. doi:10.1016/j.jcrysgro.2006.11.051.
[44] H.K. Kim, J.M. Lee, Low resistance nonalloyed Al-based ohmic contacts on n-ZnO:Al, Superlattices Microstruct. 42 (2007) 255–258. doi:10.1016/j.spmi.2007.04.054.
[45] J.J. Chen, S. Jang, F. Ren, S. Rawal, Y. Li, H.S. Kim, et al., Thermal stability of Ti/Al/Pt/Au and Ti/Au Ohmic contacts on n-type ZnCdO, Appl. Surf. Sci. 253 (2006) 746–752. doi:10.1016/j.apsusc.2006.01.012.
[46] Nazia Fathima, N. Pradeep, Jyothi Balakrishnan, Investigations of the effects of electrode geometry and mechanical stress on Antimony doped Zinc Oxide nanostructures based MSM UV photodetectors fabricated on flexible substrates, Solar Energy Materials and Solar Cells, 194 (2019) 207-214.
https://doi.org/10.1016/j.solmat.2019.02.016
[47] M. Lorenz et al, The 2016 oxide electronic materials and oxide interfaces roadmap, J. Phys. D: Appl. Phys. 49 (2016) 433001.
http://dx.doi.org/10.1088/0022-3727/49/43/433001
[48] V. E. Sandana, D. J. Rogers et al, Structural, Optical, Electrical and morphological study of transparent p-NiO/n-ZnO heterojunctions grown by PLD, Oxide-based Materials and Devices; 936410 (2015).
https://doi.org/10.1117/12.2177427